

Supplemental Information

How Does KCNE1 Regulate the Kv7.1 Potassium Channel? Model-Structure, Mutations, and Dynamics of the Kv7.1-KCNE1 Complex

Yana Gofman, Simona Shats, Bernard Attali, Turkan Haliloglu, and Nir Ben-Tal

Inventory of Supplemental Information

Figure S1, related to Figure 1, displays the evolutionary conservation profile of KCNE1 in complex with the channel according to the Kang et al. model (Kang et al., 2008).

Figure S2, related Figure 1, maps the conservation grades on the KCNE1 sequence.

Figure S6, related to Figure 1, displays the evolutionary conservation profile of the Kv7.1 model-structure.

Figure S7, related to Figure 1, shows the multiple sequence alignment of KCNE1 homologs used to calculate the conservation profile of KCNE1.

Table S1, related to Figure 2, shows the $C\beta$ - $C\beta$ distances between KCNE1-KCNQ1 residue pairs in the final model of the complex.

Movie S1, related to Figure 3, displays the motion depicted in panel A.

Movie S2, related to Figure 3, displays shows the motion depicted in panel B.

Table S2, related to Figures 3 and 4, contains the Kv7.1 hinge regions in motion I-III, in comparison to the Kv1.2 hinge regions.

Movie S3, related to Figure 4, displays the motion depicted in panel A.

Figure S9, related to Figure 5, shows the location of residues G272, L273, V310, T311 and F340 in the Kv7.1 model structure.

Movie S4, related to Figure 5, shows the motion depicted in panel A.

Figure S8, related to Figure 7, shows the hinges controlling motion II mapped on the model-structure of the complex.

Movie S5, related to Figure 8, shows the motion depicted in panel A.

Movie S6, related to Figure 8, shows the motion depicted in panel B.

Figure S3, related to Table 1, shows the contribution of the 30 slowest GNM modes to the overall motion of the Kv7.1 tetramer.

Figure S4, related to Table 1, displays mean-square fluctuations of the Kv7.1 tetramer in the three slowest GNM modes.

Figure S5, related to Table 1, shows mean-square displacement of the channel alone and in complex with four KCNE1 subunits according to the GNM and ANM modes.

Elastic Network Models

Supplemental Experimental Procedures

Supplemental References

Supplementary Information Tables

TABLE S1, related to Figure 2. The $C\beta$ - $C\beta$ distances between KCNE1-KCNQ1 residue pairs in the final model of the complex (presented in Å). In the case of G40 the distances were measured from the $C\alpha$. These pairs were verified against data from disulfide mapping studies, and the residues in each pair are separated by a distance of less than 15Å in the final model. The last column details the location of the interacting pairs, either in a loop, a TM segment (TM) or at the end of a TM segment (TM end).

| Pair | The final model | Location |
|----------|-----------------|---------------|
| G40/T144 | 12.7 | Loop/TM end |
| G40/I145 | 9 | Loop/TM end |
| G40/Q147 | 13 | Loop/Loop |
| K41/T144 | 13.9 | TM end/TM end |
| K41/I145 | 9.3 | TM end/TM end |
| K41/Q147 | 14.6 | TM end/loop |
| L42/V324 | 7 | TM end/TM end |
| E43/W323 | 5.7 | TM end/TM end |
| A44/V141 | 6.2 | TM/TM |

TABLE S2, related to Figures 3 and 4. Matching GNM modes of the Kv7.1 channel with the corresponding modes of Kv1.2 (Yehekel et al., 2010) that share similar hinges. The first column shows hinges in Kv7.1, and the second column shows hinges in the Kv1.2 channel (Yehekel et al., 2010). The third column shows the Kv7.1 positions corresponding to the Kv1.2 hinges of the second column; if the hinges are the same in Kv7.1 and Kv1.2, the same position appears in columns 1 and 3. The last column describes the involvement of each Kv7.1 hinge (first column) in diseases. LQTS1 - long QT syndrome 1; JLNS - Jervell and Lange-Nielsen syndrome; AF - atrial fibrillation.

| Kv7.1 GNM1,2+3 | Kv1.2 GNM3 | Corresponding position in Kv7.1 | Disease association |
|-------------------|------------|------------------------------------|--|
| Q147 | C181 | V141 | |
| A208 | V261 | I204 | R192P is involved in LQTS1(Napolitano et al., 2005) |
| I235 | R297 | R231 | I235N is involved in LQTS1(Choi et al., 2004; Tester et al., 2005) |
| Q260-262 | M325-L328 | R259-L262 | E261D is involved in JLNS(Tester et al., 2005); E261K(Donger et al., 1997), L262V(Napolitano et al., 2005) are involved in LQTS1 |
| T312-G316 | T373-D379 | T311-D317 | T312I(Tester et al., 2005), I313M(Tanaka et al., 1997), G314S(Chouabe et al., 1997)/C(Chen et al., 2003)/D(Tester et al., 2005)/A(Shimizu et al., 2004), Y315S(Donger et al., 1997)/C(Tester et al., 2005), G316R(Tester et al., 2005) are involved in LQTS1 |
| F340-A346 | I402-V410 | F340-G348 | A341E(Wang et al., 1996)/V(Tester et al., 2005), L342F(Chouabe et al., 1997; Donger et al., 1997), P343S(Napolitano et al., 2005), A344E/V(Tester et al., 2005), G345E(Tester et al., 2005)/R(van den Berg et al., 1997) are involved in LQTS1 |

| Kv7.1 GNM4 | Kv1.2 GNM4 | Corresponding position in Kv7.1 | Disease association |
|----------------|------------|---------------------------------|--|
| L137 | V178 | I138 | L137P is involved in LQTS1 |
| A152-T153 | F223 | F157 | |
| F232-M238 | P265 | A208 | I235N is involved in LQTS1(Chouabe et al., 1997; Donger et al., 1997) |
| I282 | V301 | I235 | |
| Y299 | L341-F348 | F275-I282 | |
| W323-G325 | V390 | I328 | G325R is involved in LQTS1(Tanaka et al., 1997) |
| Kv7.1 GNM5,6+7 | Kv1.2 GNM5 | Corresponding position in Kv7.1 | Disease association |
| V129 | L182 | L142 | |
| F167-G168 | T216 | - | G168R is involved in LQTS1(Tester et al., 2005) |
| I204-V206 | I254-T269 | P197-V212 | I204M(Napolitano et al., 2005)/F(Tester et al., 2005) is involved in LQTS1 |
| R249-V262 | L321 | V255 | L250H(Itoh et al., 1998), L251P(Deschenes et al., 2003), V254M(Tester et al., 2005) E261K(Donger et al., 1997), L262V(Napolitano et al., 2005) are involved in LQTS1; E261D is involved in JLNS(Tester et al., 2005) |
| I313-G316 | T373-G376 | T311-G314 | I313M(Tanaka et al., 1997), G314S(Chouabe et al., 1997)/C(Chen et al., 2003)/D(Tester et al., 2005)/A(Shimizu et al., 2004), Y315S(Donger et al., 1997)/C(Tester et al., 2005), G316R(Tester et al., 2005) are involved in LQTS1 |
| G345 | A403 | A341 | G345E(Tester et al., 2005)/R(van den Berg et al., 1997) is involved in LQTS1 |

Supplementary Information Figures

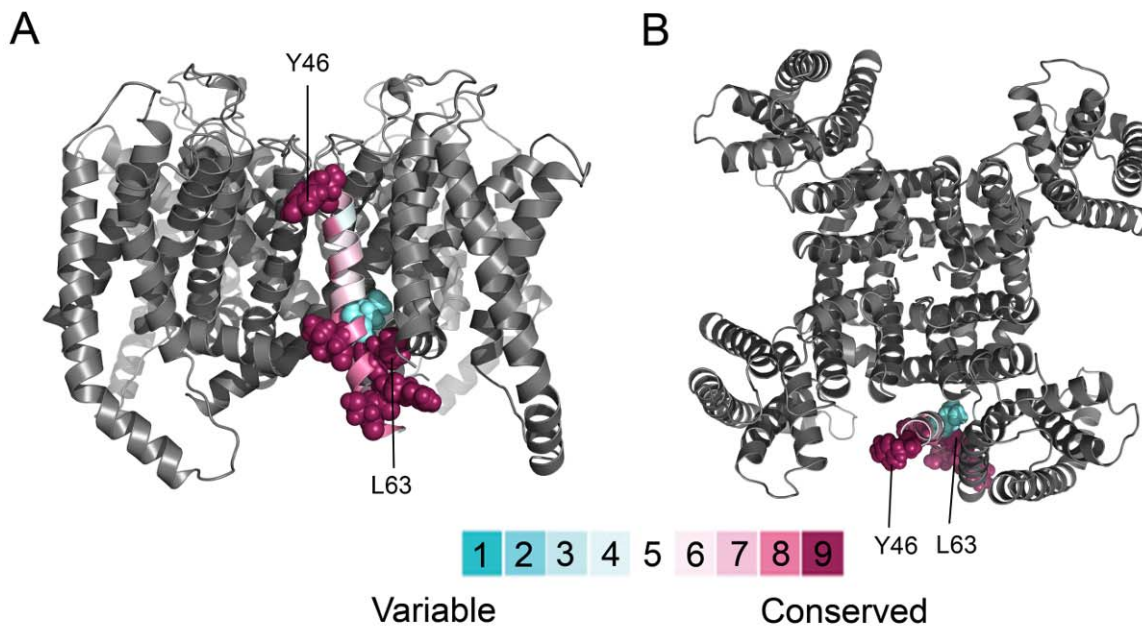


Figure S1, related to Figure 1. Extracellular (*A*) and side (*B*) views of the evolutionary conservation profile of KCNE1 in complex with the channel according to the Kang et al. model (Kang et al., 2008). The channel tetramer is in grey, and the KCNE1 model is colored by conservation grades according to the color-coding bar, with variable-through-conserved corresponding to turquoise-through-maroon. The most variable residues (score 2 – none of the residues in this region was assigned a score of 1), namely L59, and the most conserved residues (score 9), namely Y46, I61, L63, R67 and S68, are displayed as space-filled atoms. It is evident that variable residues of KCNE1 are located at the interaction interface with the channel, a conformation that is in conflict with the typical conservation pattern. KCNE1 residues Y46 and L63, mutations in which are described here, are labeled.

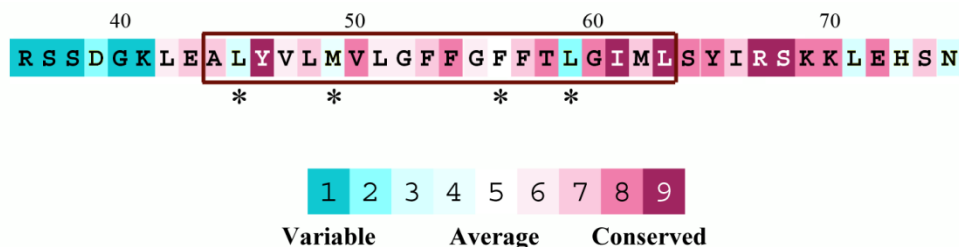


Figure S2, related to Figure 1. Mapping of the ConSurf conservation grades of Figures 1 and S1 on the KCNE1 sequence. Conservation is shown using the color-coding bar, i.e. the highly variable and highly conserved residues are shown in turquoise and maroon, respectively. The brown rectangle represents the location of the TM helical segment in the model-structure. The residues marked by asterisks are more variable than the rest. All these residues face the lipids in our model-structure of the Kv7.1-KCNE1 complex, but three of them, namely L45, F56 and L59, are in direct contact with Kv7.1 in the Kang et al. model (Kang et al., 2008).

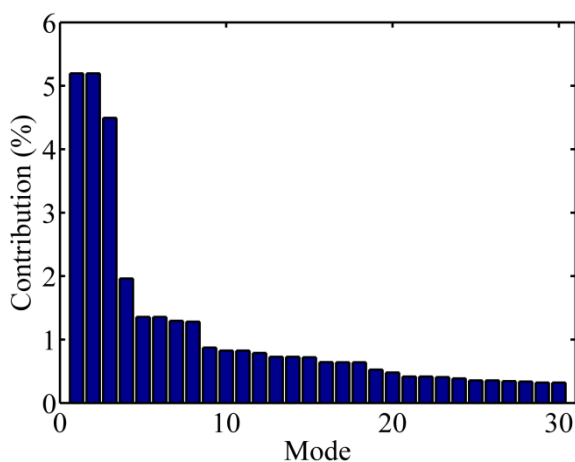


Figure S3, related to Table 1. The contribution of the 30 slowest GNM modes to the overall motion of the Kv7.1 tetramer. The percentage of contribution was estimated as the weight of the frequency of a specific mode n , calculated considering the frequencies of all N modes ($100\lambda_n/\lambda_{N-1}$). Modes 1 and 2 share the same eigenvalue, as do modes 5 and 6. We studied here the 8 slowest modes, each of which contributes over 1%.

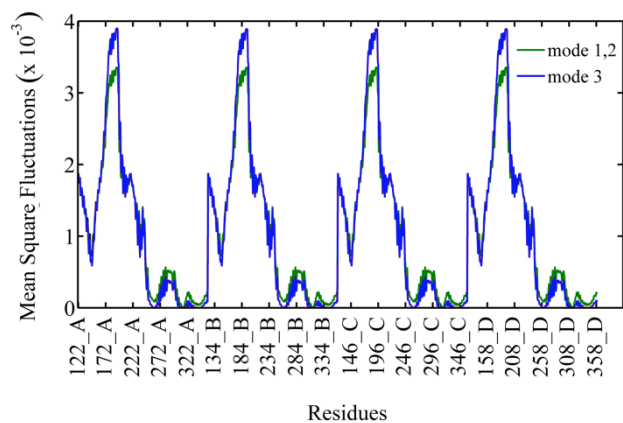


Figure S4, related to Table 1. Mean-square fluctuations of the Kv7.1 tetramer in the three slowest GNM modes. The shape of the third mode (blue) fits the profile of the average of modes 1 and 2 (green).

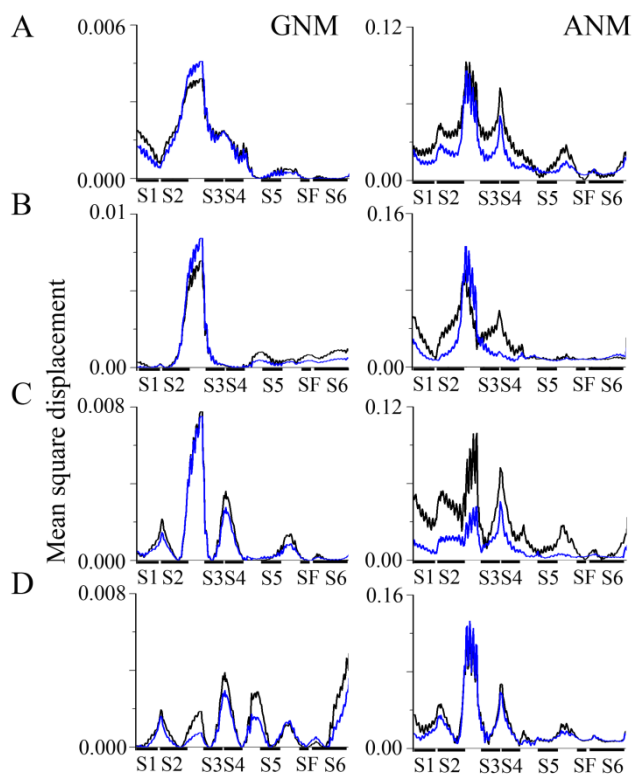


Figure S5, related to Table 1. Mean-square displacement of the channel alone (black curves) and in complex with four KCNE1 subunits (blue curves) according to the GNM and ANM modes. The modes of motion are grouped as described in Table 1: (A) Motion I; (B) Motion II; (C) Motion III; (D) Motion IV. The locations of the TM helices and the selectivity filter (SF) are marked on the x-axis. The fluctuations of one chain of the homotetrameric channel are presented, since the fluctuations of all four Kv7.1 chains are identical. The overall shape of the fluctuations is mostly preserved upon KCNE1 binding in both elastic models.

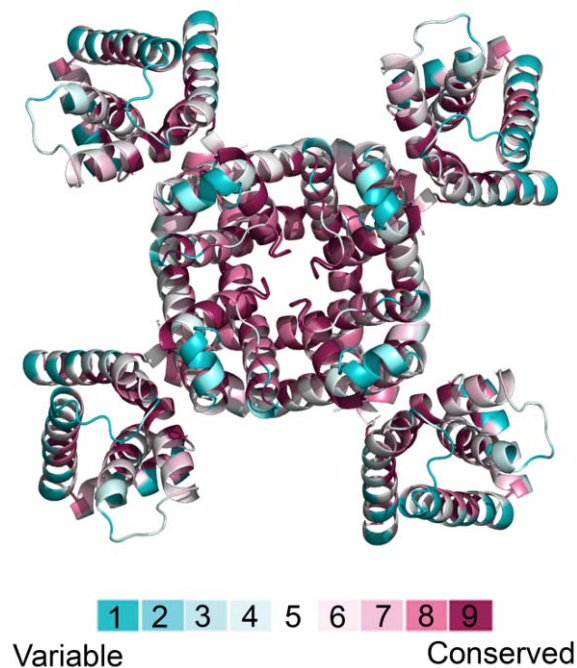


Figure S6, related to Figure 1. ConSurf (Ashkenazy et al., 2010) analysis of the Kv7.1 homology model of Smith and colleagues (Smith et al., 2007) supports the accuracy of the model. An extracellular view of the channel is colored by conservation grades according to the color-coding bar, with variable-through-conserved corresponding to turquoise-through-maroon.

Variable residues face lipids or are located in the loops, whereas conserved residues are located in the channel core, as expected.

```

gi|148231562 EEDNDNDAYIMLLIMIFYGCLAGGLIAYTRSRKQ-ESKN
gi|74008603 TSAGKDDAYIMLLIMIFYACLAGGLIAYTRSRNLVDVKD
gi|10946898 TSAGKNDAYIMLLIMIFYACLAGGLIAYTRSRKLVKAD
gi|194228201 TSAGKDDAYIMLLIMIFYACLAGGLIAYTRSRKLVKAD
gi|118150860 TSAGKDDAYIMLLIMIFYACLAGGLIAYTRSRKLVKAD
gi|109131902 TSAGKDDAYIMLLIMIFYACLAGGLIAYTRSRKLVKAD
gi|62898173 TSAGKDDAYIMLLIMIFYACLAGGLIAYTRSRKLVKAD
gi|148228535 KEHRHDNAYIMLFLVFLFAATVGSLLIAYTRSRKVV-DKRS
gi|224044131 HGGRNANAYIMLFLVMTLFAATVGSLLIAYTRSRKVV-DKRS
gi|149570042 GLGRDDNSYIMLFLVMFLFAVTVGSLLIAYTRSRKVV-DKRS
gi|50731409 RAGRDDNAYIMLFLVMTLFAATVGSLLIAYTRSRKVV-DKRS
gi|126327853 LLGRDDNSYIMLFLVMFLFAVTVGSLLIAYTRSRKVV-DKRS
gi|149719645 LPGRDDNSYIMLFLVMFLFAVTVGSLLIAYTRSRKVV-DKRS
gi|109107909 LPGRDDNSYIMLFLVMFLFAVTVGSLLIAYTRSRKVV-DKRS
gi|10181220 LPGRDDNSYIMLFLVMFLFAATVGSLLIAYTRSRKVV-DKRS
gi|281353151 LPGRDDNSYIMLFLVMFLFAATVGSLLIAYTRSRKVV-DKRS
gi|47522996 LPGRDDNSYIMLFLVMFLFAATVGSLLIAYTRSRKVV-DKRS
gi|57102546 LPGRDDNSYIMLFLVMFLFAATVGSLLIAYTRSRKVV-DKRS
gi|47224825 DRSDDGNAYIMLIVVSYFYGVFLGIMLGYFRSKLR-EKRR
gi|130492410 SGGSDNNAYIMIVVSYFYGVFLGIMLGYLRTRKR-EKRR
gi|225707444 SGESDGKAYIMLIVMSFYGVFLGIMLGYVRSKRR-EKRR
gi|213513794 TDKSYGNAYIMIFIVISFYGVFLGIMLGYVRSKRR-EKRR
gi|149634072 QSSGSGNEYIMLIVMSFYGIFLIGIMLGYVKSRR-EPKS
gi|126338342 SIGSGSEYIMLVMSFYGIFLIGIMLGYMKSRR-EKKS
gi|224059988 TEKNNSNEYIMLIVMSFYGIFLIGIMLGYMKSRR-EKSS
gi|118095023 TEKNNGNEYIMLIVMSFYGIFLIGIMLGYMKSRR-EKTS
gi|125630723 SGGSHGNEYIMLVMSFYGIFLIGIMLGYMKSRR-EKKA
gi|47058974 NSGGNGNEYIMLVMSFYGIFLIGIMLGYMKSRR-EKKS
gi|10946658 NSGGNGNEYIMLVMSFYGVFLGIMLGYMKSRR-EKKS
gi|22028392 NSGGNGNEYIMLVMSFYGVFLGIMLGYMKSRR-EKKS
gi|148225272 GSGNGNEYIMLVMSFYGIFLIGIMLGYMKSRR-EKKS
gi|109101239 GSGNGNEYIMLVMSFYGIFLIGIMLGYMKSRR-EKKS
gi|17978829 GSGNGNEYIMLVMSFYGIFLIGIMLGYMKSRR-EKKS
gi|21913154 SGSSNGNEYIMLVMSFYGIFLIGIMLGYMKSRR-EKKS
gi|57111251 SESGNGNEYIMLVMSFYGIFLIGIMLGYMKSRR-EKKS
gi|149711532 SGGNGNEYIMLVMSFYGIFLIGIMLGYMKSRR-EKKS
gi|149637420 AAENFSYIIMLVMMGMFSPFIIIVAIMSTVKSRR-ERPD
gi|118083866 DAENFYVIIIMLVMMGMFSPFIIIVAIMSTVKSRR-EHKS
gi|126325241 NAENFYVIIIMLVMMGMFSPFIIIVAIMSTVKSRR-EHSN
gi|19424314 DAENFYVIIIMLVMMGMFSPFIIIVAIMSTVKSRR-EHSQ
gi|19882205 DAENFYVIIIMLVMMGMFSPFIIIVAIMSTVKSRR-EHSQ
gi|109065428 DAENFYVIIIMLVMMGMFSPFIIIVAIMSTVKSRR-EHSN
gi|149742389 DAENFYVIIIMLVMMGMFSPFIIIVAIMSTVKSRR-EHSN
gi|116004387 DAENFYVIIIMLVMMGMFSPFIIIVAIMSTVKSRR-EHSN
gi|194040892 DAENFYVIIIMLVMMGMFSPFIIIVAIMSTVKSRR-EHSN
gi|27151626 -----YVIIIMLVMMGMFSPFIIIVAIMSTVKSRR-EHSN
gi|74001416 DAENFYVIIIMLVMMGMFSPFIIIVAIMSTVKSRR-EHSN
gi|281345139 DAENFYVIIIMLVMMGMFSPFIIIVAIMSTVKSRR-EHSN
gi|149408819 KSKFDNAYIMLFLVFLFAATVGSLLIAYTRSRKLVKAD
gi|118083876 GSTGGSLEIMLVMMVGLFGFPTVGMFNIRARRL-EDSH
gi|224097098 GSASDSLAIMLVMLLGLFGFPTVGMFNIRARRL-QGPR
gi|224097102 -----MLLQARTGFPTVGMFNIRARRL-QGPR
gi|147899362 IKSFDEMEVIMLLLVGFFGFFFTGIMSYIRSKKL-EHSG
gi|47207945 -----IMLVVGMFSPFIIIVAIMSTVKSRR-EHSG
gi|126325447 ---DAGLEVIMLMLVGLFGFPTVGMFNIRARRL-EHSH
gi|157954436 LGDDGQMEAIMLMLVGLFGFPTVGMFNIRARRL-EHSH
gi|149637414 RTTPDHLEAIMLMLVGLFGFPTVGMFNIRARRL-EHSH
gi|6685655 LRDDGKLEAIMLMLVGLFGFPTVGMFNIRARRL-EHSH
gi|455861 LRDDGKLEAIMLMLVGLFGFPTVGMFNIRARRL-EHSH
gi|149742385 SNEDGKLEAIMLMLVGLFGFPTVGMFNIRARRL-EHSH
gi|22209087 RSDGKLEAIMLMLVGLFGFPTVGMFNIRARRL-EHSH
gi|194385608 RSSDGKLEAIMLMLVGLFGFPTVGMFNIRARRL-EHSH
hKCNE1|sp|P1538 RSSDGKLEAIMLMLVGLFGFPTVGMFNIRARRL-EHSH
gi|154707797 RSDDGKLEAIMLMLVGLFGFPTVGMFNIRARRL-EHSH
gi|114683988 RSDDGKLEAIMLMLVGLFGFPTVGMFNIRARRL-EHSH
gi|197097388 RSDDGKLEAIMLMLVGLFGFPTVGMFNIRARRL-EHSH
gi|154707795 RSDDGKLEAIMLMLVGLFGFPTVGMFNIRARRL-EHSH
gi|154707801 RSDDGKLEAIMLMLVGLFGFPTVGMFNIRARRL-EHSH
gi|109065415 RSDDGKLEAIMLMLVGLFGFPTVGMFNIRARRL-EHSH
gi|74001418 GRDDSQLAAIMLMLVGLFGFPTVGMFNIRARRL-EHSH
gi|57163739 GGDDSQLAAIMLMLVGLFGFPTVGMFNIRARRL-EHSH
gi|281338851 GGNDGQLAAIMLMLVGLFGFPTVGMFNIRARRL-EHSH
gi|6981124 LRDDSKLEAIMLMLVGLFGFPTVGMFNIRARRL-EHSH
gi|6680528 LRDDSKLEAIMLMLVGLFGFPTVGMFNIRARRL-EHSH
gi|194040894 GHDDGKLAAIMLMLVGLFGFPTVGMFNIRARRL-EHSH
gi|118151402 GHEDGKLAAIMLMLVGLFGFPTVGMFNIRARRL-EHSH

```

Y46

L63

Figure S7, related to Figure 1. The multiple sequence alignment of KCNE1 homologs used to calculate the conservation profile of KCNE1. The homologs were collected from the NR database (Sayers et al., 2011) using PSI-BLAST (Altschul et al., 1997). Redundant sequences (>99% sequence identity) were discarded, and the resultant 76 sequences, all from the KCNE

family, were aligned using MUSCLE (Edgar, 2004). Only the modeled segment of KCNE1, i.e., residues 36-75, and the corresponding sequences of the homologous proteins are shown. Positions Y46 and L63, which we mutated, are highlighted.

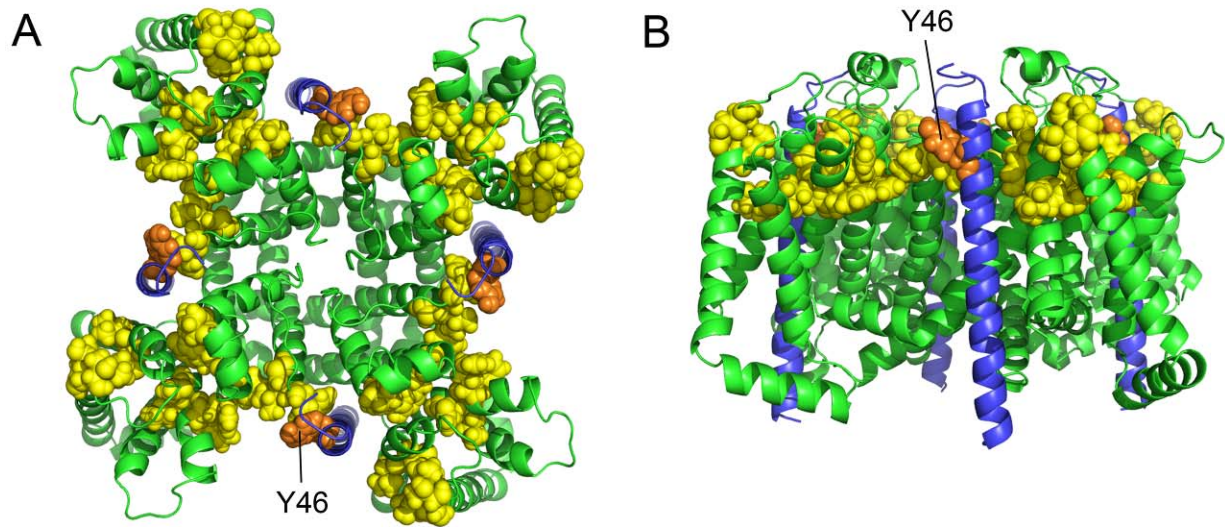


Figure S8, related to Figure 7. Hinges controlling motion II mapped on the model-structure of the complex: (A) extracellular view, (B) side view. The channel is green and KCNE1 is blue. The hinge residues of motion II are shown as yellow space-filled atoms. KCNE1 Y46 is shown as orange space-filled atoms. Clearly, the hinge residues are in close proximity to each other, creating a cluster, and KCNE1 Y46 is a part of this cluster.

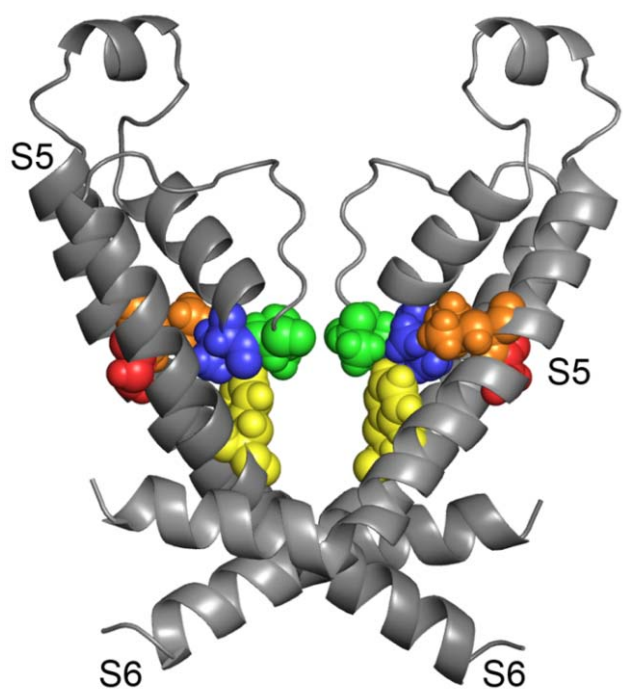


Figure S9, related to Figure 5. The location of residues G272 (red), L273 (orange), V310 (blue), T311 (green) and F340 (yellow) in the Kv7.1 model structure. Segments S5 and S6 of two diagonally-opposite chains are presented. Residues G272, L273, V310, T311 and F340 are shown as space-filled atoms. These five residues are in close proximity to each other, creating a cluster.

Supplementary Information Movies legends

Movie S1, related to Figure 3. Motion I - conformations predicted by ANM mode 4, corresponding to GNM modes 1,2 and 3 (Table 1). The model-structure is shown in ribbon representation and viewed from an extracellular perspective. The mode depicts alternate slanting of VSD pairs from diagonally-opposite monomers towards the pore.

Movie S2, related to Figure 3. Motion III - conformations predicted by ANM mode 8, corresponding to GNM modes 5,6 and 7 (Table 1). The model-structure is shown in ribbon representation and viewed from an extracellular perspective. The mode depicts alternate slanting of VSD pairs from diagonally-opposite monomers towards the pore.

Movie S3, related to Figure 4. Motion II - conformations predicted by ANM mode 1, corresponding to GNM mode 4 (Table 1). The model-structure is shown in ribbon representation and viewed from an extracellular perspective. The mode depicts swinging of VSDs, while the pore domain appears to be essentially stationary.

Movie S4, related to Figure 5. Motion IV - conformations predicted by ANM mode 5, corresponding to GNM mode 8 (Table 1). The model-structure is shown in ribbon representation and viewed from an extracellular perspective. In this mode the channel is divided into two dynamic domains, connected by hinges located approximately along the membrane mid-plane. The mode depicts rotation of the two dynamic domains in opposite directions.

Movie S5, related to Figure 8. Inactivation of KcsA. ANM-predicted motion, related to KcsA inactivation, is presented. The ANM calculation was performed using HingeProt (Emekli et al., 2008). The structure is shown in ribbon representation and viewed from the side. For clarity, only two diagonally-opposite chains are presented. The α -carbons of E71 and D80 are shown as red space-filled atoms.

Movie S6, related to Figure 8. Inactivation of Kv7.1. Motion predicted by ANM mode 8 and related to voltage-gated slow inactivation of Kv7.1 is shown. The model structure is shown in ribbon representation and viewed from the side. For clarity, only two diagonally-opposite chains are presented. The α -carbons of E295 and D317 are shown as red space-filled atoms.

Elastic network models

In the GNM calculations the protein structure was simplified into α -carbon atoms and treated as an elastic network of nodes connected by hookean springs of uniform force constant γ . Two nodes i and j were assumed to display Gaussian fluctuations around their equilibrium position if the distance between them was below the (commonly used) cutoff of 10 Å. The inter-node contacts were then defined by an $N \times N$ Kirchoff matrix $\mathbf{\Gamma}$, where N is the number of amino acids in the protein. The correlation between the fluctuations of two nodes i and j , $\Delta\mathbf{R}_i$ and $\Delta\mathbf{R}_j$, respectively, was calculated as follows:

$$\langle \Delta\mathbf{R}_i \Delta\mathbf{R}_j \rangle = (3k_B T / \gamma) [\mathbf{\Gamma}^{-1}]_{ij} = (3k_B T / \gamma) \sum_k [\lambda_k^{-1} \mathbf{u}_k \mathbf{u}_k^T]_{ij} \quad (1)$$

where \mathbf{u}_k and λ_k are, respectively, the k -th eigenvector and k -th eigenvalue of $\mathbf{\Gamma}$, k_B is the Boltzmann constant, and T is the absolute temperature; $k_B T / \gamma$ was taken as 1 Å². Overall, Eq. 1 predicts the mean-square displacement of each residue (node) when $i=j$, and when $i \neq j$ it predicts the correlations between the fluctuations of residues i and j as a superimposition of $N-1$ eigenmodes. λ_k is proportional to the k -th mode frequency, the inverse of which gives the relative contribution of this mode to the protein's overall structural motion. The minima in the obtained fluctuation profile for a given mode suggest possible hinge points that coordinate the cooperative motions between structural elements in this mode.

In contrast to isotropic GNM, ANM determines the direction of fluctuations. Here $\mathbf{\Gamma}$ is replaced by the $3N \times 3N$ Hessian matrix \mathbf{H} , the elements of which are the second derivatives of the inter-node potential described by Eq. 1, with a cutoff of 15 Å. The correlation between $\Delta\mathbf{R}_i$ and $\Delta\mathbf{R}_j$ was decomposed into $3N-6$ modes and calculated as follows:

$$\langle \Delta \mathbf{R}_i \Delta \mathbf{R}_j \rangle = (3k_B T / \gamma) \text{tr}[\mathbf{H}^{-1}]_{ij} = (3k_B T / \gamma) \sum_k \text{tr}[\lambda_k^{-1} \mathbf{u}_k \mathbf{u}_k^T]_{ij} \quad (2)$$

where $\text{tr}[\mathbf{H}^{-1}]_{ij}$ is the trace of the ij -th submatrix $[\mathbf{H}^{-1}]_{ij}$ of \mathbf{H}^{-1} . The eigenvectors allowed us to identify alternative conformations sampled by the individual modes, simply by adding/subtracting the eigenvectors to/from the equilibrium position in the respective modes. Thus, being an anisotropic model, ANM provides information on the directions of the motions in 3D, while GNM is more realistic with respect to the mean-square fluctuations and the correlation between fluctuations (Bahar et al., 2010).

Several studies have demonstrated that the first few slowest GNM modes, assigned the lowest frequencies, are implicated in protein function (Bahar et al., 2010; Bahar and Rader, 2005). The least mobile residues suggested by these modes play key mechanical roles, such as being hinge centers or controlling the cooperative movements of domains. Therefore, we focused on the eight GNM modes identified as slowest on the basis of the distribution of eigenvalues; these modes were responsible for approximately 22% of the overall motion (Figure S3). The superimposition of the residues' mean square displacement predicted by GNM and ANM revealed the correspondence between the two elastic network models. Thus, using ANM, we were able to determine the direction of fluctuations characterized by GNM.

Experimental procedures

The mutations of human KCNE1 were constructed using standard PCR techniques, using the Pfu DNA polymerase (Promega). The mutants were entirely sequenced using a DNA automatic sequencer. Human KCNE1 DNA (*wt* and mutants) were linearized by BamHI enzyme

(Promega); human KCNQ1 DNA (*wt*) were linearized by Not1 enzyme (Promega). Capped complementary RNAs (cRNAs) were transcribed from linearized human KCNE1 by T3 RNA polymerases and from linearized human KCNQ1 with T7 RNA polymerases (mMessage mMachine, Ambion). The cRNAs were quantified by UV spectroscopy (Nanodrop), and its integrity and concentration were verified by running an aliquot on a formaldehyde agarose gel. Channel expression into *Xenopus* oocytes and electrophysiology were performed as previously described (Gibor et al., 2007). Current signals were filtered at 0.2 kHz and digitized at 1 kHz. The holding potential was -80mV. The reversal potential of the membrane, according to the Nernst-equation, was calculated to be $V_{rev} = -81.4\text{mV}$.

$$E_{K^+} = \frac{RT}{ZF} \times \ln \frac{[K^+]_o}{[K^+]_i} \quad (3)$$

Where R = gas constant, T = temperature, Z = valence, F = Faraday's constant and $[K^+]_o = 4\text{mM}$, $[K^+]_i = 100\text{mM}$. In order to subtract the leak off line from the currents obtained in the I - V protocol, we changed the resistance at the -80mV step pulse of the trace obtained (which is about the E_{rev}) in order to zero the current. Then, the other voltage-step currents were leak-subtracted accordingly, using the Ohm's law. Data analysis was performed using the Clampfit program (pCLAMP 10.2, Molecular Devices), Microsoft Excel (Microsoft), Prism (Graphpad). For a measure of deactivation kinetics, a single exponential fit was applied to the tail currents and measured from +40mV prepulse at -60 mV tail potential according to:

$$f(t) = \sum_{i=1}^n A_i e^{-t/\tau_i} + C \quad (4)$$

Because of the complex activation kinetics of the currents, including a sigmoidal delay, a rough estimate of the activation kinetics, $T_{1/2}$ act was calculated from the macroscopic current and measured at +40mV. $T_{1/2}$ act is the time at which the current amplitude is half-activated. To analyze the voltage dependence of I_{KS} channel activation, a single exponential fit was applied to the tail currents (-60 mV tail potential) and extrapolated to the beginning of the repolarizing step. Chord conductance (G) was calculated by using the following equation:

$$G = I / (V - V_{rev}) \quad (5)$$

Where I corresponds to the current, and V_{rev} corresponds to the calculated reversal potential. G was estimated at various test voltages V and, then, normalized to a maximal conductance value, G_{max} , calculated at +40 mV.

Voltage-dependent activation curves were fitted by the Boltzmann equation:

$$G / G_{max} = 1 / (1 + \exp^{(V_{50} - V) / s}) \quad (6)$$

Where V_{50} is the voltage at which the current is half-activated, and s is the slope factor. To analyze the voltage dependence of I_{KS} channel activation, G was deduced from tail currents as above. All data were expressed as mean \pm SEM. Statistically significant differences between the *wt* and the mutants were assessed by Student's t-test.

Supporting References

- Altschul, S.F., Madden, T.L., Schaffer, A.A., Zhang, J., Zhang, Z., Miller, W., and Lipman, D.J. (1997). Gapped BLAST and PSI-BLAST: a new generation of protein database search programs. *Nucleic Acids Res.*, *25*, 3389-3402.
- Ashkenazy, H., Erez, E., Martz, E., Pupko, T., and Ben-Tal, N. (2010). ConSurf 2010: calculating evolutionary conservation in sequence and structure of proteins and nucleic acids. *Nucleic Acids Res.*, *38 Suppl*, W529-533.
- Bahar, I., Lezon, T.R., Bakan, A., and Shrivastava, I.H. (2010). Normal mode analysis of biomolecular structures: functional mechanisms of membrane proteins. *Chem. Rev.*, *110*, 1463-1497.
- Bahar, I., and Rader, A.J. (2005). Coarse-grained normal mode analysis in structural biology. *Curr. Opin. Struct. Biol.*, *15*, 586-592.
- Chen, S., Zhang, L., Bryant, R.M., Vincent, G.M., Flippin, M., Lee, J.C., Brown, E., Zimmerman, F., Rozich, R., Szafranski, P., *et al.* (2003). KCNQ1 mutations in patients with a family history of lethal cardiac arrhythmias and sudden death. *Clin Genet*, *63*, 273-282.
- Choi, G., Kopplin, L.J., Tester, D.J., Will, M.L., Haglund, C.M., and Ackerman, M.J. (2004). Spectrum and frequency of cardiac channel defects in swimming-triggered arrhythmia syndromes. *Circulation*, *110*, 2119-2124.
- Chouabe, C., Neyroud, N., Guicheney, P., Lazdunski, M., Romey, G., and Barhanin, J. (1997). Properties of KvLQT1 K⁺ channel mutations in Romano-Ward and Jervell and Lange-Nielsen inherited cardiac arrhythmias. *EMBO J*, *16*, 5472-5479.
- Deschenes, D., Acharfi, S., Pouliot, V., Hegele, R., Krahn, A., Daleau, P., and Chahine, M. (2003). Biophysical characteristics of a new mutation on the KCNQ1 potassium channel (L251P) causing long QT syndrome. *Can J Physiol Pharmacol*, *81*, 129-134.
- Donger, C., Denjoy, I., Berthet, M., Neyroud, N., Cruaud, C., Bennaceur, M., Chivoret, G., Schwartz, K., Coumel, P., and Guicheney, P. (1997). KVLQT1 C-terminal missense mutation causes a forme fruste long-QT syndrome. *Circulation*, *96*, 2778-2781.
- Edgar, R.C. (2004). MUSCLE: multiple sequence alignment with high accuracy and high throughput. *Nucleic Acids Res.*, *32*, 1792-1797.
- Emekli, U., Schneidman-Duhovny, D., Wolfson, H.J., Nussinov, R., and Haliloglu, T. (2008). HingeProt: automated prediction of hinges in protein structures. *Proteins*, *70*, 1219-1227.
- Gibor, G., Yakubovich, D., Rosenhouse-Dantsker, A., Peretz, A., Schottelndreier, H., Seebohm, G., Dascal, N., Logothetis, D.E., Paas, Y., and Attali, B. (2007). An inactivation gate in the selectivity filter of KCNQ1 potassium channels. *Biophys. J.*, *93*, 4159-4172.
- Itoh, T., Tanaka, T., Nagai, R., Kikuchi, K., Ogawa, S., Okada, S., Yamagata, S., Yano, K., Yazaki, Y., and Nakamura, Y. (1998). Genomic organization and mutational analysis of KVLQT1, a gene responsible for familial long QT syndrome. *Hum Genet*, *103*, 290-294.
- Kang, C., Tian, C., Sonnichsen, F.D., Smith, J.A., Meiler, J., George, A.L., Jr., Vanoye, C.G., Kim, H.J., and Sanders, C.R. (2008). Structure of KCNE1 and implications for how it modulates the KCNQ1 potassium channel. *Biochemistry*, *47*, 7999-8006.

Napolitano, C., Priori, S.G., Schwartz, P.J., Bloise, R., Ronchetti, E., Nastoli, J., Bottelli, G., Cerrone, M., and Leonardi, S. (2005). Genetic testing in the long QT syndrome: development and validation of an efficient approach to genotyping in clinical practice. *JAMA*, *294*, 2975-2980.

Sayers, E.W., Barrett, T., Benson, D.A., Bolton, E., Bryant, S.H., Canese, K., Chetvernin, V., Church, D.M., DiCuccio, M., Federhen, S., *et al.* (2011). Database resources of the National Center for Biotechnology Information. *Nucleic Acids Res.*, *39*, D38-51.

Shimizu, W., Horie, M., Ohno, S., Takenaka, K., Yamaguchi, M., Shimizu, M., Washizuka, T., Aizawa, Y., Nakamura, K., Ohe, T., *et al.* (2004). Mutation site-specific differences in arrhythmic risk and sensitivity to sympathetic stimulation in the LQT1 form of congenital long QT syndrome: multicenter study in Japan. *J Am Coll Cardiol*, *44*, 117-125.

Smith, J.A., Vanoye, C.G., George, A.L., Jr., Meiler, J., and Sanders, C.R. (2007). Structural models for the KCNQ1 voltage-gated potassium channel. *Biochemistry*, *46*, 14141-14152.

Tanaka, T., Nagai, R., Tomoike, H., Takata, S., Yano, K., Yabuta, K., Haneda, N., Nakano, O., Shibata, A., Sawayama, T., *et al.* (1997). Four novel KVLQT1 and four novel HERG mutations in familial long-QT syndrome. *Circulation*, *95*, 565-567.

Tester, D.J., Will, M.L., Haglund, C.M., and Ackerman, M.J. (2005). Compendium of cardiac channel mutations in 541 consecutive unrelated patients referred for long QT syndrome genetic testing. *Heart Rhythm*, *2*, 507-517.

van den Berg, M.H., Wilde, A.A., Robles de Medina, E.O., Meyer, H., Geelen, J.L., Jongbloed, R.J., Wellens, H.J., and Geraedts, J.P. (1997). The long QT syndrome: a novel missense mutation in the S6 region of the KVLQT1 gene. *Hum Genet*, *100*, 356-361.

Wang, Q., Curran, M.E., Splawski, I., Burn, T.C., Millholland, J.M., VanRaay, T.J., Shen, J., Timothy, K.W., Vincent, G.M., de Jager, T., *et al.* (1996). Positional cloning of a novel potassium channel gene: KVLQT1 mutations cause cardiac arrhythmias. *Nat Genet*, *12*, 17-23.

Yehekel, A., Haliloglu, T., and Ben-Tal, N. (2010). Independent and cooperative motions of the Kv1.2 channel: voltage sensing and gating. *Biophys. J.*, *98*, 2179-2188.